

Physics Design and Scaling of Elise

E. P. Lee, R. O. Bangerter, C. F. Chan, A. Faltens, J. Kwan, E. Henestroza, K. Hahn, P. Seidl, J. J. Barnard, A. Friedman, D. P. Grote, and W. M. Sharp

This article was submitted to
International Symposium on Heavy Ion Inertial Fusion, Princeton, NJ, September
6-9, 1995

August 1, 1995

U.S. Department of Energy

Lawrence
Livermore
National
Laboratory

DISCLAIMER

This document was prepared as an account of work sponsored by an agency of the United States Government. Neither the United States Government nor the University of California nor any of their employees, makes any warranty, express or implied, or assumes any legal liability or responsibility for the accuracy, completeness, or usefulness of any information, apparatus, product, or process disclosed, or represents that its use would not infringe privately owned rights. Reference herein to any specific commercial product, process, or service by trade name, trademark, manufacturer, or otherwise, does not necessarily constitute or imply its endorsement, recommendation, or favoring by the United States Government or the University of California. The views and opinions of authors expressed herein do not necessarily state or reflect those of the United States Government or the University of California, and shall not be used for advertising or product endorsement purposes.

This is a preprint of a paper intended for publication in a journal or proceedings. Since changes may be made before publication, this preprint is made available with the understanding that it will not be cited or reproduced without the permission of the author.

This report has been reproduced
directly from the best available copy.

Available to DOE and DOE contractors from the
Office of Scientific and Technical Information
P.O. Box 62, Oak Ridge, TN 37831
Prices available from (423) 576-8401
<http://apollo.osti.gov/bridge/>

Available to the public from the
National Technical Information Service
U.S. Department of Commerce
5285 Port Royal Rd.,
Springfield, VA 22161
<http://www.ntis.gov/>

OR

Lawrence Livermore National Laboratory
Technical Information Department's Digital Library
<http://www.llnl.gov/tid/Library.html>

Physics Design and Scaling of Elise

E.P. Lee, R.O. Bangerter, C.F. Chan, A. Faltens, J. Kwan,
E. Henestroza, K. Hahn, and P. Seidl

Accelerator and Fusion Research Division
Lawrence Berkeley National Laboratory
University of California
Berkeley, California 94720

J.J. Barnard, A. Friedman, D.P. Grote, and W.M. Sharp

Lawrence Livermore National Laboratory
Livermore, California 94550

August 1995

PHYSICS DESIGN AND SCALING OF ELISE*

**E.P. Lee, R.O. Bangerter, C.F. Chan, A. Faltens, J. Kwan,
E. Henestroza, K. Hahn, and P. Scidl**

Lawrence Berkeley National Laboratory, 1 Cyclotron Road, Berkeley, CA 94720

J.J. Barnard, A. Friedman, D.P. Grote, and W.M. Sharp
Lawrence Livermore National Laboratory, Livermore, CA 94550

Abstract

Elise is an electrostatically focused heavy-ion accelerator being designed and constructed at Lawrence Berkeley Laboratory. The machine is intended to be the first half of the four-beam Induction Linac Systems Experiment (ILSE), which ultimately will test the principal beam dynamics issues and manipulations of induction heavy-ion drivers for inertial fusion. Elise will use an existing 2 MeV injector and will accelerate space-charge-dominated pulses to greater than 5 MeV. The design objective of Elise is to maximize the output beam energy within the fixed project budget while allowing for adequate beam diagnostics, flexibility in the acceleration schedule, and beam parameters suitable for ILSE and the experimental program.

We review the design equations and "rules of thumb" used for choosing beam and lattice parameters for heavy-ion induction accelerators, and we discuss incorporating these relations in a spreadsheet program that generates internally consistent lattice layouts and acceleration schedules. These designs have been tested using a one-dimensional (1-D) particle simulation code, SLIDE, a 3-D fluid/envelope code, CIRCE, and a 3-D particle-in-cell code WARP3D. Sample results from these calculations are presented. Results from these dynamics codes are also shown illustrating sensitivities to beam and lattice errors and testing various strategies for longitudinal confinement of the beam ends.

1. Introduction

Elise is an electrostatically focused heavy-ion induction accelerator being designed and constructed at Lawrence Berkeley National Laboratory. The machine will be built in a way that

* Work performed under the auspices of the U.S. Department of Energy at LBL under Contract No. DE-AC03-76SF00098 and at LLNL under contract W-7405-ENG-48.

allows future expansion into the full Induction Linac Systems Experiment (ILSE) configuration which includes beam combining and magnetic focusing. Elise will demonstrate beam manipulations and address other beam dynamics issues associated with a heavy ion driver for inertial fusion.

The design objective of Elise is to optimize the beam current density and the total energy while allowing for adequate beam diagnostics, flexibility in the acceleration schedule, and beam parameters suitable for ILSE and other experimental programs. Since Elise has many features similar to that of driver-scale accelerators, the project will produce valuable information (both technical and cost data) for designing a fusion driver.

Elise will have an array of four ESQ (electrostatic quadrupole) focusing channels capable of transporting up to, and for some scenarios more than, a total of 3.2 A of beam current. With a line charge density similar to that of heavy ion drivers, Elise will accelerate a 1 μ s beam pulse of K^+ ions from an initial energy of 2 MeV to a final energy of more than 5 MeV. Initially, only one beam channel will be used during nominal Elise operation. Eventually, for ILSE upgrade, a new injector will produce 4 beams that will be combined into 1 before entering a magnetically focused accelerating section for further acceleration to more than 10 MeV.

Elise is intended to approximate as realistically as possible the front end of an induction linac driver. The electric quadrupole geometry and operating voltages and the resultant transportable beam are all at full driver scale, and except for the necessarily shorter pulse length, would provide directly useful information for the future. In a driver, the electric focusing section would be a few hundred meters in length, throughout most of which the beam pulse is almost of constant physical length and constant line charge density. Part of Elise will duplicate such operation. At the entrance to the driver, some tens of meters are devoted to the process of launching the bunch in a manner which avoids heating it in the longitudinal phase plane; this space is insignificant on the driver scale. For Elise, a gentle starting section would correspond to a significant fraction of the entire

machine, yet it is important to devise starting scenarios for a driver which can be investigated experimentally in Elise. The machine is consequently being designed to enable exploration of several candidate scenarios, all of which are acceptable in preserving beam quality, but will have various economic consequences.

2. Elise Technical Design Parameters

Approximate design and performance goal parameters are listed below in table 1. In some cases (e.g., final current), these exceed commissioning requirements. They will also vary dependent on the mode of operation and experimental objectives.

insert TABLE 1

3. ESQ Injector and Matching Section

On the basis of reliability, driver scalability, and beam specifications an ESQ[1] design was selected for the injector. A one-beam prototype of the ESQ injector has been built and tested at LBNL. The prototype provides up to at least 0.8 Amperes of 2 MeV K⁺ ions, equivalent to a line charge density of 0.25 $\mu\text{C/m}$, at a low normalized emittance ($<1 \text{ mm-mr}$), repetition rate of 1 Hz and pulse length of 1 μs . The ESQ injector consists of a diode followed by a sequence of quadrupoles arranged to focus and accelerate the beam at the same time. A schematic of the injector is shown in Fig. 1. The ESQ is generally a long machine with correspondingly low gradients. The secondary electrons are swept out by the large transverse fields, which reduces significantly the breakdown risks. In addition, the sources in an ESQ are generally smaller than those matched to a high gradient column, so the intrinsic emittance is lower. The ESQ is also attractive because of its scaling; it has the potential advantage of operating at energies somewhat higher than 2 MeV, since the critical issues of emittance growth in an ESQ tend to center in the transition from the diode to the first accelerating quadrupoles.

The diode consists of a hot alumino-silicate source with a large curved emitting surface surrounded by a thick "extraction electrode." An extraction pulser switches the source from -80 kV

to +80 kV relative to the extraction electrode during beam turn-on. The pulser voltage profile has a 0.5 μ s rise and fall time, with a 1.0 μ s flat top. The EGUN [2] code was used in the design of the diode.

The design of the ESQ injector was based on the three-dimensional PIC (particle-in-cell) codes WARP3D[3] and ARGUS[4] running in a steady state mode. A full 3-D PIC simulation code was required to incorporate the beam space-charge-field as well as the self-consistent fields from the accelerating quadrupoles, including their "inter-digital" structure (cantilevered electrode rods). The "inter-digital" structure of the electrostatic quadrupoles could enhance the aberrations. The resulting kinematic distortions lead to S-shaped phase spaces, which, if not corrected, will lead eventually to emittance growth. These beam aberrations can be minimized by increasing the injection energy and/or strengthening the beam focusing. The parameters of the design represent optimal choices to have a proper balance between breakdown risks and emittance growth. With the design diode voltage of 750 kV, a small normalized emittance (0.6 mm-mr) was obtained. The intrinsic normalized emittance is 0.4 mm-mr.

The experimental results from the injector matched the code predictions[5]. Measurements of the transverse phase space distribution have shown excellent agreement with WARP3D calculations. Good agreement was found as well in the current profile with the transient longitudinal dynamics of the beam in the ESQ simulated by running GYMNOS[6] and WARP3D in time dependent modes.

The matching section (Figure 2) was designed to reduce the beam size from the injector to the size of the main transport channel. Using WARP3D, a simulated beam which was created in the injector and transported through the matching section. With the rise and fall time of 0.5 micro-s from the injection pulser, the rise and fall at the end of the matching section is between 0.3 and 0.5 micro-s, short enough to alleviate concerns about beam expansion in the matching section from the lack of axially confining fields.

FIGURE 2

4. ESQ Transport Dynamics in the Induction Accelerator

The transportable beam current in an ESQ channel is governed by the aperture radius and the voltages applied to the ESQ. The scaling is such that optimum beam current per unit cross-sectional area is obtained by using an array of ESQ channels with small aperture radius. However, there is a lower practical limit to the aperture radius due to the minimum beam clearance imposed by random errors in beam steering and accelerator alignments. In the present design, Elise beam channels will have a constant aperture radius of 2.33 cm and a nearly constant quadrupole voltage of about ± 60 kV.

Based on optimizing the “Figure-of-Merit,” defined as the maximum beam line charge per unit area, the optimum aperture radius is determined to be $b = 2.33$ cm. The peak beam radius (a) is related to the aperture radius by the equation:

$$b = 1.25a + c$$

The coefficient 1.25 is due to a limitation from the image force from the electrodes and the beam clearance c is obtained from an estimate of the beam steering random error and accelerator alignment limits which are expected to be in the order of a few mm. The maximum line charge density could be more than doubled if the clearance allowance can be reduced from 1.0 cm to less than 0.2 cm. The electrode radius (R_e) is determined by setting the dodecapole component of the focusing electric field to zero, which means the ratio of the electrode radius to the aperture radius is 1.146 (or $\approx 8/7$).

ESQ spark-down tests (at LBNL) have shown that the maximum voltage for the ESQ is proportional to the square root of the spacing between quadrupole electrodes. An ESQ with $b = 2.3$ cm and $R_e = 2.53$ cm broke down at 230 kV between the quadrupole electrodes. As a rule of thumb, we set the normal operating point at below 50% of the spark-down threshold value.

Based on these rules, we found that the optimum value of b is 2.33 cm and the ESQ voltage, V_q , is 118 kV (or ± 59 kV).

The next important dimension to determine is the lattice half period length (L) and the maximum associated transportable line charge density, λ . These are accurately determined from the matched envelope relations:

$$\cos \sigma_0 = 1 - \frac{\eta^2 \left(1 - \frac{2}{3}\eta\right)}{2} \left(\frac{E'}{2T}\right)^2 L^4$$

$$\frac{\lambda}{4\pi\epsilon_0 T} \left(\frac{2L}{a}\right)^2 = 2(1 - \cos \sigma_0) \left[1 + \eta \left(\frac{E'}{2T}\right) \frac{L^2}{4} \left(1 - \frac{\eta}{2}\right)\right]^{-2}.$$

Here σ_0 is the undepressed phase advance per lattice period, η is the field occupying fraction of the ESQ, $E' = V_q/b^2$ is the quadrupole field gradient, and T is kinetic energy (expressed in electron volts).

Occupancy factor η can be approximated according to the relation:

$$\eta = (L - 6.0 \text{ cm}) / L.$$

The 6.0 cm spacing is made up of the “dead space” between the ESQ electrodes and the end plates (which is necessary for holding the quadrupole voltage), the end plates thickness (≈ 1 cm), and a 2.0 cm acceleration gap between the end plates of neighboring ESQ modules (for typically 100 kV acceleration). Obviously η grows with L ; typical values of η start from ≈ 0.7 at the beginning and exceed 0.8 at the end of Elise.

According to the above equation for the half lattice period L , and using a 75° undepressed phase advance (85° is considered the upper limit of stable operation), we found L to be 20.8 cm at $T=2$ MeV beam energy. Everything else being kept constant, L is proportional to the square root of beam energy (a pretty good approximation for slowly varying η). On the other hand, once the dimensions such as b and L 's are fixed, the undepressed phase advance can be raised up to 85° if the quadrupole voltage V_q can reach ± 65.5 kV without incurring spark-downs.

Ideally to avoid a mismatch of the beam radius, the half-lattice period L should vary as the square root of beam energy and inversely as η , thus L becomes longer after each acceleration gap.

Depending on the cost of engineering and fabricating ESQ's, it may be worthwhile to consider using blocks of ESQ's that have the same L within each block and accept the consequence of a minor mismatch. The net result is a reduction in the transportable beam current compared to the case of continuous changing L in each period. For example, assuming no beam head-to-tail energy variation, a single-stage L will transport 50%, a 3-stage will have 73% and a 10-stage one will have 93% of the beam current found in the continuous limit. (The advantage of a 10-stage or continuous limit may not be this high if the acceleration schedule imposes a significant head-to-tail energy variation). At present, the estimated cost of fabricating ESQ's with continuously varying L is about \$350K (35%) higher than ESQ's with only 2 different L values. Thus, Elise will most likely use continuously varying L .

Voltages on the ESQ electrodes can be arranged either in the bipolar or unipolar configurations. In the former case, ± 59 kV potentials are applied to the two pairs of electrodes whereas in the latter case +118 kV and ground potentials are used. The two cases produce a small difference in the beam dynamics as long as the beam energy is much higher than the focusing potential. Basically, the unipolar design has twice the acceleration voltage across an accelerating gap but only half as many accelerating gaps (there is a non-accelerating gap between each pair of accelerating gaps). The emittance growth resulting from the bigger kicks is undesirable but tolerable in the unipolar case. In the end, the selection between bipolar and unipolar quadrupoles relies mostly on engineering and economics reasons.

Since the estimated costs for both systems are the same within 5%, we have chosen the bipolar design because of its lower risk and higher flexibility. The ability to use cantilevered mounting of the ESQ's makes it possible to achieve a reasonable axial packing of core material.

In order to prevent beam elongation, a small head-to-tail velocity tilt is applied, i.e. tail is moving faster than the head, hence the tune at the beam head is higher than that of the tail and tail beam is fatter than the head. For a constant aperture but aperiodic transport channel, it is appropriate to define matching to mean a constant maximum envelope radius. The gentle deviation from the matched envelope due to velocity tilt is unimportant as shown in simulations, as

long as the envelope stays in the dynamic aperture mentioned above. Envelope codes predict additional ± 2.0 mm mismatch oscillation at the beam ends due to the velocity tilt.

It may be desirable to have the same voltages on all the quadrupoles, so that several quadrupoles are driven by a common power supply. For a given acceleration schedule, it is straight forward to design a lattice satisfying the above criteria.

5. Longitudinal Dynamics and Acceleration Schedule

Assuming that the transverse beam dynamics is handled properly by the appropriate ESQ focusing field and the correctly scaled half-length periods, we examine the problem of longitudinal beam dynamics.

The acceleration schedule in Elise is closely tied to the lattice design. As discussed elsewhere [7] and in section 4 of this report, the present design has the length of quadrupoles increasing along the lattice approximately in proportion with the beam velocity, while keeping the same voltage on all quadrupoles. This choice avoids transverse mismatches by maintaining a constant average focusing strength. Although the beam velocity as a function of position is in principle quite flexible, the choice made in Elise is to maximize the packing density of acceleration cores, consistent with breakdown limits, access for pulsed-power feeds and diagnostics, and preservation of some modularity. The juggling of parameters to optimize cost and performance is handled by the MATHEMATICA optimization code discussed in section 6. The present design has average acceleration voltages varying somewhat erratically between 55.7 kV and 153.75 kV, with gaps for diagnostics in place of two cells. Despite the irregular acceleration, simulations using the envelope/fluid code CIRCE indicate that the beam remains near transverse equilibrium along its length.

For any acceleration schedule, there remains considerable flexibility in longitudinal compression of the beam. CIRCE simulations indicate that compression is best achieved by imposing a smooth velocity variation or “tilt” along the beam, while balancing the beam axial space-charge field on the average by “ear” fields applied in selected acceleration gaps. “Ears” are

small voltages superimposed on the original one at the beginning and end of the pulse. They are produced by fast-responding cores and pulsers. A velocity tilt is introduced by appropriate time variation of the accelerating voltage in one or more gaps, and theoretical work by Kim and Smith [8] indicates that waveform giving self-similar compression of the beam current has a nearly linear voltage variation with time. The amount of velocity tilt that can be imposed is limited by three considerations: (1) The undepressed phase advance per lattice period σ_0 is approximately proportional to the inverse square of the beam velocity for electric focusing, so the requirement that σ_0 at the beam head must remain less than 90° either limits the velocity tilt or forces a reduction in the average focusing strength, driving up the beam size. (2) Any velocity tilt complicates beam steering because the transverse kick from electric or magnetic dipoles depends on velocity. (3) The maximum acceleration field, usually at the beam tail, plus any ear field there, which is also maximum at the tail, cannot exceed the breakdown limit in any cell. The first constraint is the most salient for Elise, typically limiting velocity tilt to about 20%. The second constraint is also important because the Elise beam will ultimately be merged with three others in the beam combiner of the Induction Linac Systems Experiments (ILSE). Since the combiner uses electric dipoles to bend the four beams, its velocity acceptance is limited to a few percent at the final Elise energy. The third constraint is typically more important as a limit on the spacing between ear cells than on the allowable velocity tilt.

Elise is being designed with sufficiently large induction cores to allow several compression scenarios to be tested. The simplest choice is to impose no velocity tilt, in which case the Elise beam would have a constant duration in the absence of axial space charge and, with space charge, would increase in duration by about 15%. Since the average beam energy increases from 2 MeV to 5.7 MeV, the beam length nearly doubles in this case. A simple prescription for imposing a substantial tilt is to apply triangular acceleration pulses, with zero voltage at the head and the nominal cell voltage at the tail. The maximum velocity difference along the beam is then controlled by the number of cells with time-varying voltage relatively small, it gives the largest peak velocity tilt for a given compression and therefore limits the allowable focusing strength. An

Fig. 4. Total pulse length is about 1.8 μ s (down from 2.2 μ s), with an average peak current 0.9 amp. There is also a large energy tilt, with the head at 5.2 MeV, and the tail at 6.5 MeV.

Figure 3

Figure 4

6. Cost Optimization

Although the physics of Elise design is the main topic of this paper, the design has also been optimized so that the performance of the machine (measured in total pulse energy) has been maximized subject to the constraints of a maximum allowable cost, and also subject to the requirement of meeting the goals of the physics experiments. In order to obtain a design, an approximate cost algorithm was developed which included relevant engineering constraints and data. A Mathematica-based design code was written (in addition to an Excel spreadsheet code), which then laid down each half-lattice period, determining core and quadrupole lengths, evaluating beam parameters, and calculating incremental costs for each of these components. Cost optimizations were then made which scanned over such parameters as length and width of the amorphous iron cores, ion energy and pulse duration.

6.1 Design Algorithm

We outline the basic algorithms used in the code below. Many of the parameters of the machine and their justification have already been mentioned: The ion mass (39.1 amu) and charge state (+1), injected beam energy (2.0 MeV) and normalized emittance (1.0×10^{-6} m-rad), initial current (0.78 A), pipe radius for each beam (2.33 cm), and quadrupole voltage (118 kV) are set by previous considerations.

Each induction core is an annular cylinder of ferromagnetic material. The beam acts like the secondary of a one turn transformer as it threads the core. The core allows a voltage increment V_c for a duration Δt_V which can be shown by use of Faradays law to satisfy:

$$V_c \Delta t_V = \Delta B A_c f_p.$$

Here ΔB is the magnetic flux swing in the ferromagnetic material, f_p is the packing fraction of the magnetic material, (~ 0.75), and $A_c = (R_0 - R_i)L_c$ is the area of the core. The ferromagnetic material we have chosen for cost and efficiency considerations is METGLAS®. Note that Δt_v is the full-width-half-maximum of the voltage pulse, and that for flattop current pulse of duration Δt_i , the current rise and fall each lasts about $0.3 \mu s$, so that a $1.5 \mu s$ current flattop consumes about $2.5 \mu s$ in effective voltage pulse.

Several cores of differing inner and outer radius can be combined on a common mandrel to form a single acceleration “cell,” and several cells may be stacked longitudinally to form a “module,” enclosed in a metallic can. Present designs generally have one module per half-lattice-period. One or two core lengths are chosen to allow flexibility in adding cells. This flexibility is needed because space must be reserved at the end of each module (5.1 cm) to allow room for high voltage feed-throughs to power the electrostatic quadrupoles, and the location of these feed-throughs generally cannot be too close to the acceleration gaps between quads, nor too close to the ground plate (approximately midway between gaps). By combining different core lengths a large fraction of the longitudinal space can be utilized, avoiding excluded areas, and maximizing the number of volt-seconds per meter available for acceleration and pulse length. The algorithm which is used in the Mathematica code at each half-lattice period adds, from a selection of two cell types, the maximum core area that can be added within the constraint imposed by the length of the half-lattice period and the constraint that the module end does not lie too close to the acceleration gap.

The voltage on each core has an upper limit determined primarily by the voltage stand-off capabilities of the thyatron switch, used for initiation of the discharge of the pulse forming network, which provides the energy storage and pulse shaping of the voltage pulse. If the core is chosen so that its area results in a volt-second capability that is smaller than the product of maximum voltage times the required pulse length for the current pulse, then either the voltage must be less than the maximum voltage or the head and tail voltage must differ. The algorithm used in the optimization code adds the maximum voltage increment to the tail of the pulse, and uses whatever voltage is permissible to the head assuming a trapezoidal pulse shape. This gives a

larger velocity to the tail than to the head, which in turn causes the pulse duration to decrease, a technique which will be used in fusion drivers to compress the pulse length as the beam accelerates. In most of the optimization runs however the machine is designed using a constant current acceleration schedule, in which the pulse duration is constant. Enough flexibility exists in the designs so that the schedules described in section 5 can also be carried out. Once the energy increment is chosen, the length of the half-lattice period is determined by ensuring that the envelope of the beam remains "matched" :

$$\eta EL/\sqrt{T} = \text{const.}$$

Here η is the longitudinal occupancy of the quadrupole relative to the half-lattice period, E' is the transverse electrostatic gradient in the quadrupole, L is the half-lattice period, T is the particle kinetic energy. This condition is applied at the beginning of each quadrupole, after acceleration from the previous acceleration gap. This leads to a half-lattice period which increases approximately as the square root of the energy when the quadrupole voltage is fixed. With the energy increment and half-lattice period length determined, the analytic formulas for the beam properties at the head and tail of the pulse, such as average and maximum beam radius, and depressed and undepressed tunes may be calculated using the results of section 4. The current and line charge density are calculated at the head and the tail, ignoring space charge effects and assuming charge conservation. These assumptions lead to the current at the head of the beam which satisfies,

$$I_{h_i} \equiv \left(\frac{I_h}{1 - (L/v_h^2)(dv_h/dt)} \right)_{i-1}$$

Here I_h , V_h , and dV_h/dt are the current, velocity, and velocity time derivative, evaluated at the head of the pulse, and i indicates the number of the acceleration gap. A similar expression is used for the tail of the pulse. A uniform velocity time derivative is assumed across the pulse [$dv/dt \equiv (v_t - v_h)/(t_t - t_h)$] where subscript t indicates tail, and t is arrival time at the end of a particular acceleration gap. This formula is kinematic only, since space charge has been neglected, but for the purposes of optimization and initial design scoping the approximations are adequate. More

accurate fluid and particle codes (cf. sections 3 - 5) are used for beam studies. Simple models for the quadrupole dimensions as well as the cell and module dimensions are incorporated into the code and a graphical display of the entire machine is then generated. (See figure 5).

FIGURE 5

6.2 Costing algorithms

Algorithms for costing the three major variable costs have been incorporated into the code. These are: transport, acceleration modules, and pulsers. A simplified cost model for the quadrupole transport can be expressed as:

$$C_{\text{transport}} = C_{\text{fixed}} + C_{\text{hlp}} N_{\text{hlp}}$$

Here $C_{\text{transport}}$ is the total transport cost in dollars, and is composed of C_{fixed} , the fixed cost for developing the quad system (estimated to be ~180K\$ for a machine like Elise), plus the cost per quad C_{hlp} times the number of quads (equal to the number of half-lattice periods N_{hlp}) C_{hlp} has been estimated to be 25K\$.

The second major cost component is the cost of the acceleration modules C_{modules} which can be written in the form:

$$C_{\text{modules}} = C_{\text{mod0}} N_{\text{mod}} + C_{\text{mod1}} (R_{\text{mo}}/1\text{m})^2 N_{\text{mod}} + C_{\text{core}} N_{\text{core}} + C_{\text{MET}} p_{\text{MET}} N_{\text{cell}} U_{\text{cell}}$$

Here C_{mod0} ($\cong 3.9$ K\$) is the cost associated per module apart from costs which scale with outer module radius R_{mo} , C_{mod1} ($\cong 8.9$ K\$) is the cost associated per module which scales with R_{mo}^2 , C_{core} ($\cong 2.4$ K\$) is the cost associated with each individual core, C_{MET} ($\cong 6-14$ \$/kg) is the cost per kg of METGLAS® which includes mechanical costs which scale with accelerator weight (~ 3 \$/kg), with winding the cores ~ 3 \$/kg, and the price of METGLAS® (from 3.3 \$/kg to 8.4 \$/kg depending on core length and variety of METGLAS®). The variables N_{core} , N_{cell} , N_{mod} ,

represent the total number of cores, cells and modules, respectively, ρ_{MET} is the density of METGLAS® ($\cong 7180 \text{ kg/m}^3$) and U_{cell} is the volume of METGLAS® in each accelerating cell.

The third major cost component is the cost of pulse power C_{pulser} which has two major parts. One part arises because of the power limitations of the thyatron switches ($\sim 72 \text{ MW}$) and the associated costs per pulser, and the second part is the marginal cost per Joule of the stored energy. These can be summarized approximately as

$$C_{\text{pulser}} \cong N_{\text{cell}} U_{\text{cell}} L [C_{\text{pulW}} + C_{\text{pulJ}} (1.25/\Delta T_V)]$$

Here $C_{\text{pulW}} \cong 0.17 \text{ \$/kW}$ is the cost per kW of a 72 MW pulser, and $C_{\text{pulJ}} \cong 50 \text{ \$/J}$ is the cost per J of core energy loss, which requires energy storage in the pulse forming line making up the pulser. L is the energy loss per cubic meter of core volume associated with eddy currents and hysteresis losses and is given approximately by:

$$L \cong (400 \text{ J/m}^3) \left(\frac{\Delta B}{2T} \right)^2 \left(\frac{2\mu\text{s}}{\Delta t_V} \right)$$

The power requirements on the pulser have been assumed to be 25% larger than the energy loss in the core L divided by the effective pulse length Δt_V because of other energy loss mechanisms such as those that occur in the pulse forming line.

The total direct cost is taken to be the sum of $C_{\text{transport}}$, C_{modules} , and C_{pulser} .

6.3 Results from the cost optimization

The results of the cost study yielded insight in four areas of optimization: Core length, module outer radius, pulse duration and final ion energy. Figure 6 illustrates a series of models for different core lengths. The dollars per joule is plotted as a function of the number of cores per cell. The pulse duration is held constant in this series of curves. On a given curve, increasing the number of cores per cell increases the outer radius of the induction modules. As the core length

increases, since the volt-seconds per core and hence core area is fixed, the outer radius decreases at fixed number of cores per cell. Two observations can be made: The outer radius of the machine is optimum at about 1.0 m, while the optimum tape width occurs at 5.6" or 6.7" (or a combination of the two). An optimum in module radius occurs because as the number of cores per cell increases, the outer radius of the module increases, and although transport costs become small, because the core volume rapidly increases, so do the costs. On the other hand, when the number of cores per cell is too small, the weight of the METGLAS® becomes smaller, but the total length of the machine increases and the cost is dominated by transport costs. The optimum in length occurs because, using longer cores reduces the amount of unused spaces in-between cells increasing the longitudinal packing fraction of core material from about 0.5 for 2" cores to over 0.6 for the longer cores. Additionally, the longer cores have a substantially lower unit cost per kg (about \$3.30 /kg versus about \$8.4/kg for the 2" cores).

Another result of the cost optimization is the tradeoff between pulse duration and ion energy, when the cost of the machine is constrained. In this tradeoff it was found that if the goal is to design a machine in which the pulse energy is maximized, then increasing the pulse duration tends to win over increasing ion energy. Increasing the pulse duration requires larger and more costly cores, but because the core losses are reduced per unit core volume (because dB/dt is reduced) and the power requirements per unit core volume (proportional to $I/\Delta t v$) are reduced, the pulser requirements increase less rapidly with increasing pulse duration than with ion energy. So, for a fixed cost but maximizing pulse energy gained in the accelerator, longer pulse duration is preferred. On the other hand, because Elise is being designed to demonstrate a variety of acceleration schedules, as well as deliver maximal pulse energy, a maximum flat-top current pulse duration of about 1.5 μ s is now being considered, so that the bunch length of the beam remains a reasonably small fraction of the accelerator length, and "load and fire" scenarios as well as bunch length compression schedules can be carried out.

7. Elise Diagnostics

There will be three basic types of detector devices for the measurement of beam current and transverse beam distributions: current-measuring Faraday cups, beam slits or pinholes, and current-profile measuring harps. The Faraday cups are fairly conventional units, changing little from the types used on previous LBNL experiments such as MBE-4 and SBTE. The emittance measuring slit-harp combination will evolve from the present design of slits with cups to slits with multiple-detector arrays (harp-like constructions). Harp detectors will have 0.002 inch-thick wires and, possibly, active amplifier arrays at the detector elements. They can be fabricated with the necessary precision using electro-formed nickel elements.

At least two locations in the matching section design will allow the breaking of the vacuum system and longitudinal separation in order to insert intercepting diagnostics for the measurement of transverse phase space in two planes, and total current. The accelerator is ~14 m long, with only two non-accelerating gaps ~6.5 and ~10m downstream of the matching section.

Double-slit position and emittance measuring devices will be installed in the matching section and in a box that will move downstream as the accelerator is assembled. Some of the hardware is available from earlier experiments.

The two non-accelerating locations in the lattice are the only places where intercepting diagnostics can easily be inserted without breaking vacuum. The idea here is to measure the beam profile in two directions with a retractable slit-Faraday cup combination utilizing only the 2.0 cm gap between the quadrupole endplates. In order to minimize the possibility of breakdown between the diagnostics, and the quadrupole endplates which are held at a potential of 59-70 kV, the gap between those particular quadrupoles may be increased from 2 cm to ~4 cm. The quadrupole voltages immediately upstream and downstream would need to be adjusted somewhat to account for the break in the FODO structure.

After the accelerator has been built, double slit, or slit-harp phase space measuring devices will be inserted as needed by creating longitudinal space by breaking the vacuum between quadrupoles

and inserting the diagnostics apparatus. The accelerator is being designed so that this will take less than one day.

The accelerating voltage waveforms will be measured using a capacitive voltage divider inserted in each accelerating cell. These measurements are essential to determining the proper operation of the accelerating cells as well as for input into the longitudinal dynamics codes for evaluation of the accelerator experiments.

Data for the momentum distribution along an ion bunch is essential for the study of longitudinal beam dynamics. On MBE-4 and SBTE, these parameters were measured using an electrostatic spectrometer with an energy resolution of better than 0.5%. For Elise this technique is more difficult because the beam energies are a factor of five or more higher. Preliminary designs have been started for a magnetic analyzer that would be usable to full beam energy. This device is rather large and expensive and would probably be useful only as an end-of-accelerator diagnostic.

The investigation of an energy measurement technique that determines the ion energy by time-of-flight is in progress. At the point of measurement, the Elise beam is collimated to a pencil beam and gated to a short pulse (tens of nanoseconds). Measurement of the flight time from this point to a downstream detector (Rogowski loop if adequately sensitive, or else a Faraday cup) can yield measurements of the beam energy versus time in the pulse. This technique has the advantages of permitting measurements at any of the diagnostic locations within Elise and should be much less expensive than a magnetic spectrometer.

Figure Captions

Figure 1. ESQ Injector schematic.

Figure 2. Matching section to the Elise accelerator.

Figure 3. Pulse acceleration at constant current to 5.7 MeV.

Figure 4. Pulse acceleration with compression in time to 5.2 MeV. Note energy tilt.

Figure 5. An optimal Elise configuration of cores and quadrupoles.

Figure 6. Costs vs. core lengths for Elise.

Table 1.
Elise Technical Design Parameters

PARAMETER	UNITS	VALUE
Initial Ion Kinetic Energy	MeV	2
Initial Beam Current	Amperes	0.8
Initial Pulse Duration	Micro-seconds	1.0
Initial Beam Line Charge Density	Micro-Coulombs per meter per beam	0.25
Initial Number of Beams	none	1
Final Average Ion Kinetic Energy	MeV	5
Final Beam Current	Amperes	1.0
Final Pulse Duration	Micro-seconds	0.8
Final Beam Line Charge Density	Micro-Coulombs per meter per beam	0.2
Final Beam Energy	Joules	4
Length of Linac	meters	15
Number of Acceleration Gaps	none	51
Ion Mass Number	atomic mass units	39
Ion Charge	electron charge	+1

Figure Captions

Figure 1. ESQ Injector schematic.

Figure 2. Matching section to the Elise accelerator.

Figure 3. Pulse acceleration at constant current to 5.7 MeV.

Figure 4. Pulse acceleration with compression in time to 5.2 MeV. Note energy tilt.

Figure 5. An optimal Elise configuration of cores and quadrupoles.

Figure 6. Costs vs. core lengths for Elise.

REFERENCES

- [1] E.A. Abramyan and V.A. Gaponov, *Atomnaya Energiya* 20, 385(1966).
- [2] W.B. Herrmannsfeldt, "EGUN- An electron optics and gun design program," SLAC-Report-331, 1988.
- [3] A. Friedman, D. Grote, and I. Haber, "Three-dimensional particle simulation of heavy-ion fusion beams," *Phys. Fluids B4*, 2203(1992).
- [4] C.L. Chang, et al., "Three-Dimensional Modeling of Accelerators", Los Alamos Report, LA-11857-C, 1990.
- [5] S. Yu, et.al, "Driver-Scale Ion Injector Experiments," included in these proceedings
- [6] D.W. Hewett and D.J. Larsen, "The Best of Gymnos: a user's guide", LLNL Report, UCRL-ID-110499, May 1992.
- [7] J.W. Kwan, R.O. Bangerter, A. Faltens, C. Peters, L.L. Reginato. "Elise Plans and Progress," in these proceedings.
- [8] C.H. Kim and L. Smith, *Part. Accel.* 85, 101 (1986).
- [9] E.P. Lee, T.J. Fessenden, and L.J. Laslett, *IEEE Trans. Nuc. Science* NS-32, 2489 (1985).
- [10] E. Henestroza, HIFAR Note 379, March 1989, LBNL.
- [11] W.M. Sharp, *Proceedings of the 1995 Particle Accelerator Conference*, May 1-5, Dallas, Texas.

Figure Captions

Figure 1. ESQ Injector schematic.

Figure 2. Matching section to the Elise accelerator.

Figure 3. Pulse acceleration at constant current to 5.7 MeV.

Figure 4. Pulse acceleration with compression in time to 5.2 MeV. Note energy tilt.

Figure 5. An optimal Elise configuration of cores and quadrupoles.

Figure 6. Costs vs. core lengths for Elise.

Table 1.
Elise Technical Design Parameters

PARAMETER	UNITS	VALUE
Initial Ion Kinetic Energy	MeV	2
Initial Beam Current	Amperes	0.8
Initial Pulse Duration	Micro-seconds	1.0
Initial Beam Line Charge Density	Micro-Coulombs per meter per beam	0.25
Initial Number of Beams	none	1
Final Average Ion Kinetic Energy	MeV	5
Final Beam Current	Amperes	1.0
Final Pulse Duration	Micro-seconds	0.8
Final Beam Line Charge Density	Micro-Coulombs per meter per beam	0.2
Final Beam Energy	Joules	4
Length of Linac	meters	15
Number of Acceleration Gaps	none	51
Ion Mass Number	atomic mass units	39
Ion Charge	electron charge	+1

REFERENCES

- [1] E.A. Abramyan and V.A. Gaponov, *Atomnaya Energiya* 20, 385(1966).
- [2] W.B. Herrmannsfeldt, "EGUN- An electron optics and gun design program," SLAC-Report-331, 1988.
- [3] A. Friedman, D. Grote, and I. Haber, "Three-dimensional particle simulation of heavy-ion fusion beams," *Phys. Fluids B4*, 2203(1992).
- [4] C.L. Chang, et al., "Three-Dimensional Modeling of Accelerators", Los Alamos Report, LA-11857-C, 1990.
- [5] S. Yu, et.al, "Driver-Scale Ion Injector Experiments," included in these proceedings
- [6] D.W. Hewett and D.J. Larsen, "The Best of Gymnos: a user's guide", LLNL Report, UCRL-ID-110499, May 1992.
- [7] J.W. Kwan, R.O. Bangerter, A. Faltens, C. Peters, L.L. Reginato. "Elise Plans and Progress," in these proceedings.
- [8] C.H. Kim and L. Smith, *Part. Accel.* 85, 101 (1986).
- [9] E.P. Lee, T.J. Fessenden, and L.J. Laslett, *IEEE Trans. Nuc. Science* NS-32, 2489 (1985).
- [10] E. Henestroza, HIFAR Note 379, March 1989, LBNL.
- [11] W.M. Sharp, Proceedings of the 1995 Particle Accelerator Conference, May 1-5, Dallas, Texas.

Fig.1

1/2 pp

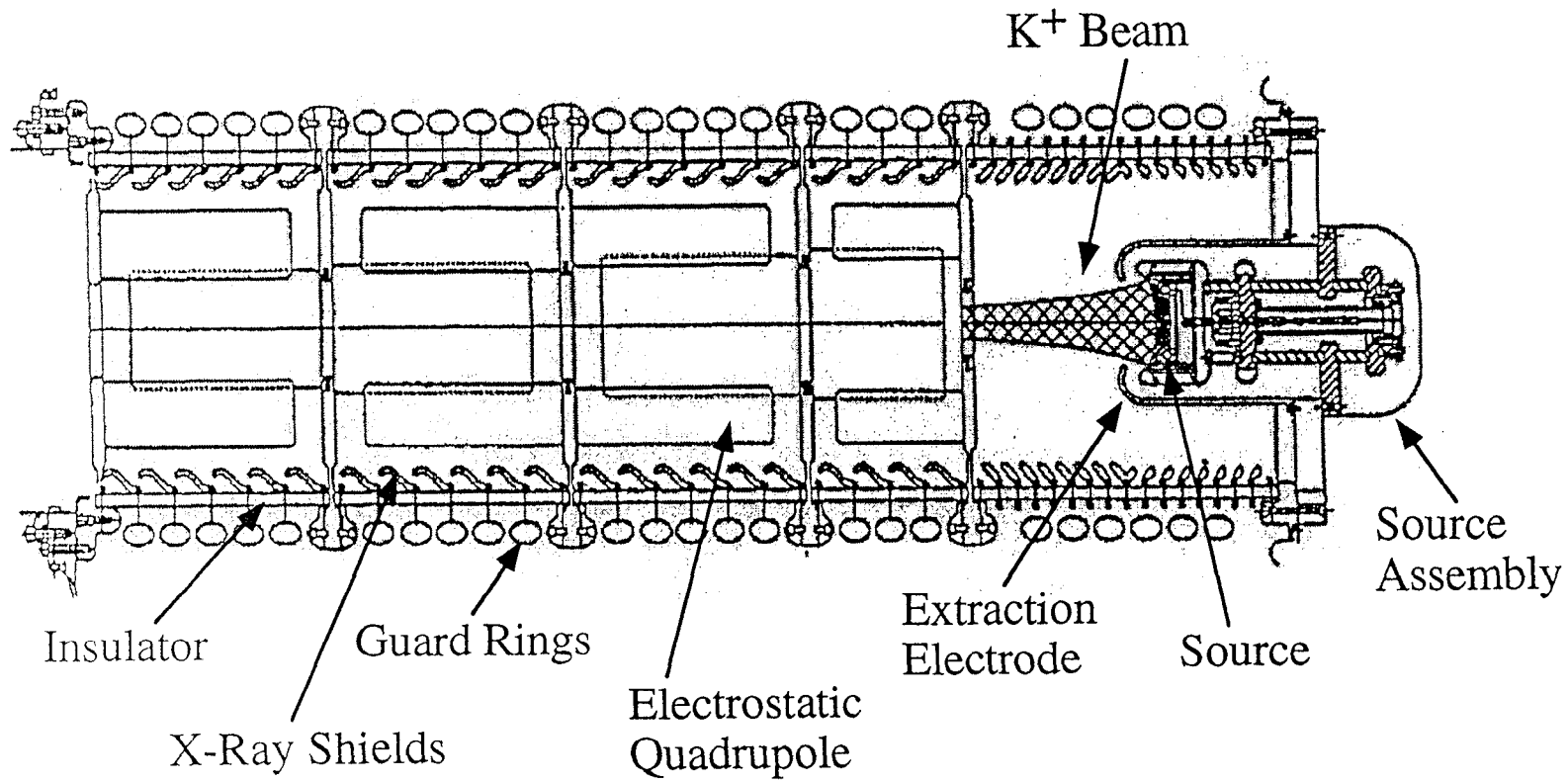


Fig. 2

1/4 pp

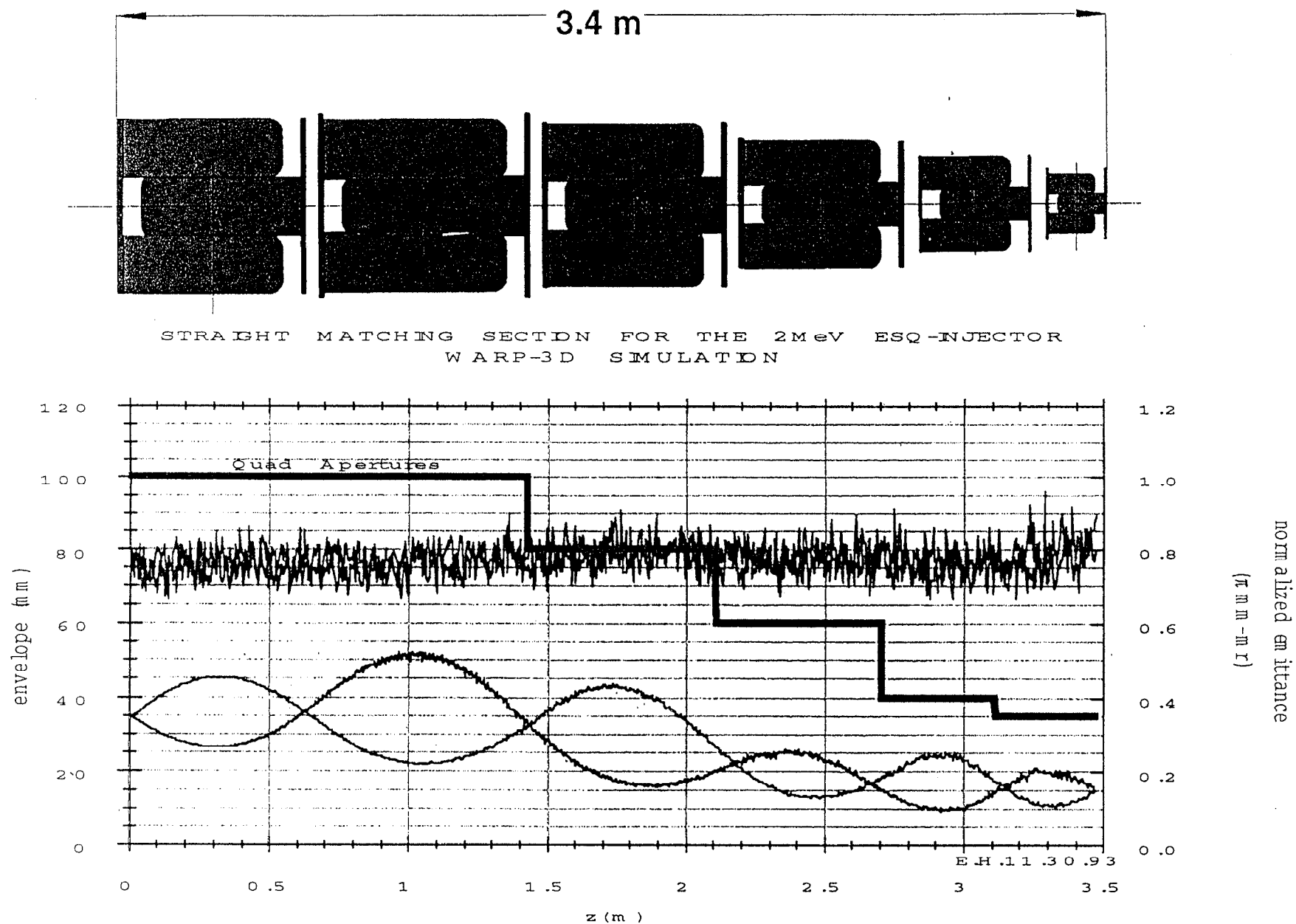


Fig. 3

1/4
1/2

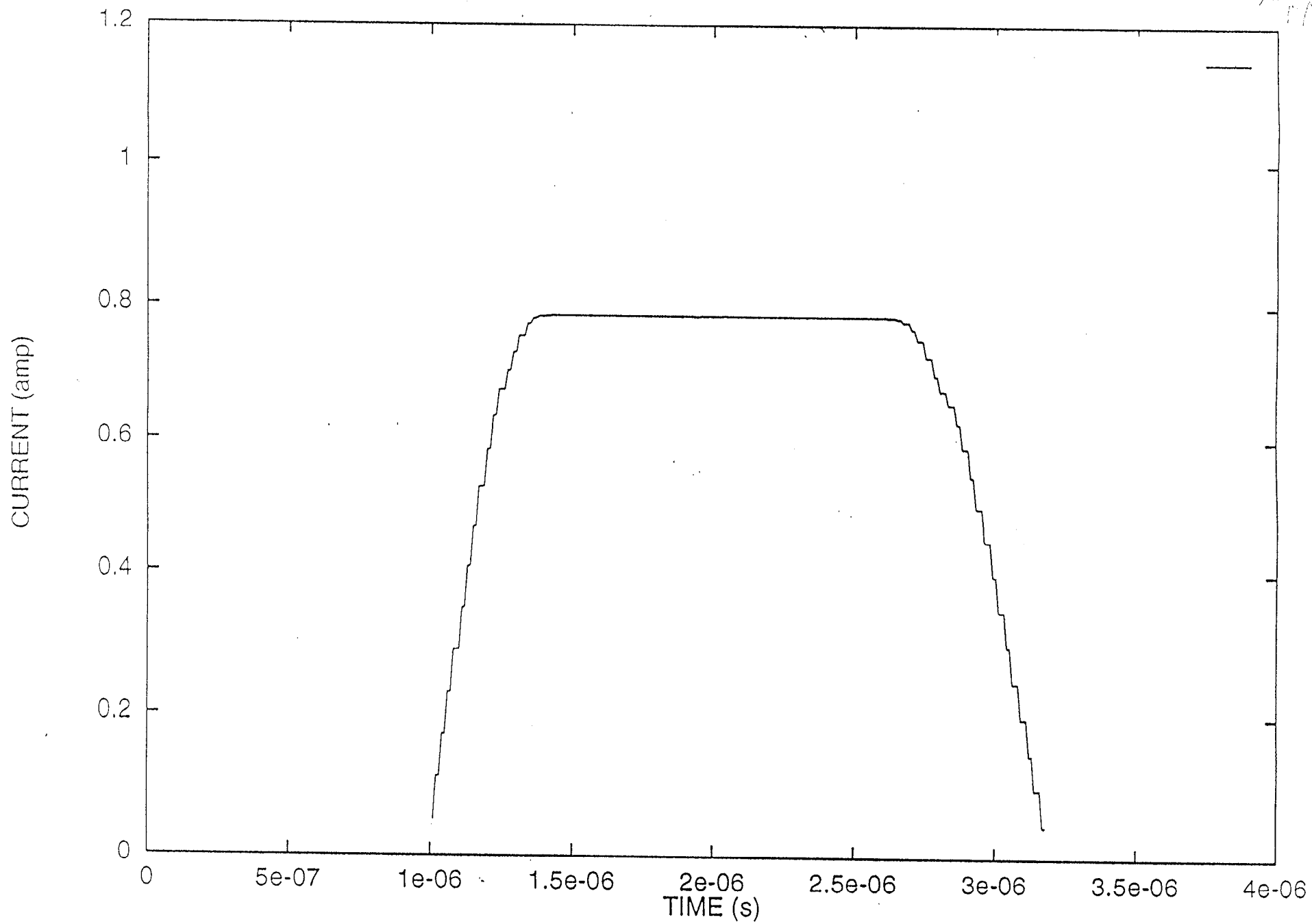


Fig. 4 $\frac{1}{4}$ pp

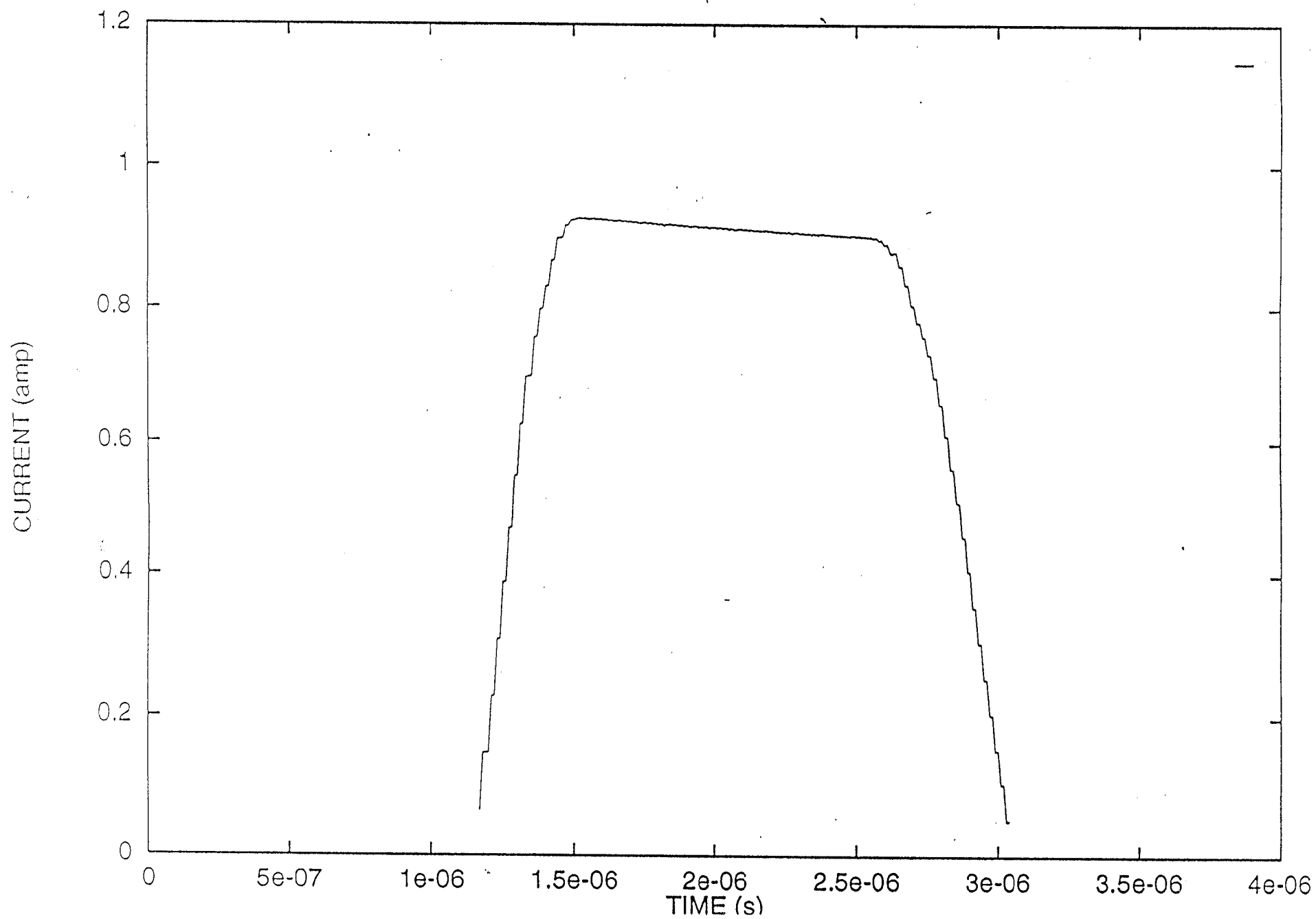


Fig. 5

$\frac{1}{2}pp$

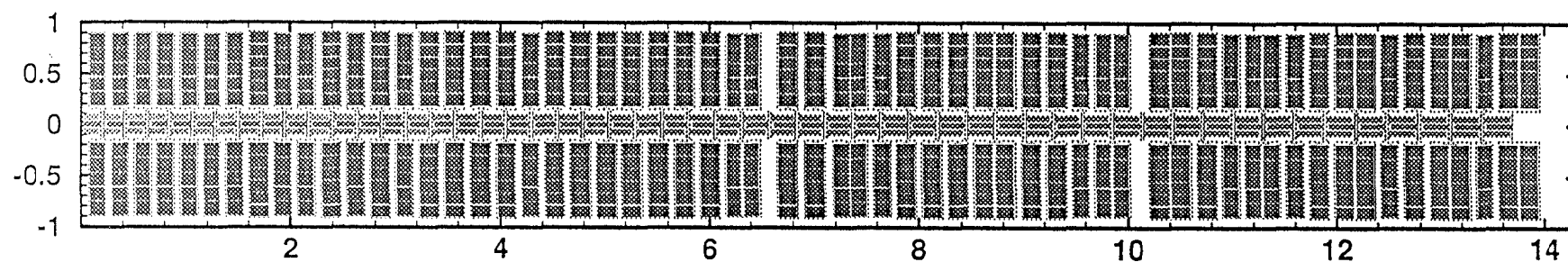


Fig. 6

1/4 pp

